Catalysis Letters
https://doi.org/10.1007/s10562-024-04778-9

Insight into the Interaction of Perovskite-Like Surfaces ($LaMnO_3$ and $LaCoO_3$) with Ar, H_2, CO, and O_2 through NAP-XPS Analysis

Juan Tapia-P.[1] · **Jaime Gallego**[2,3] · **Oscar Gamba**[4] · **Juan F. Espinal**[1]

Received: 1 March 2024 / Accepted: 3 July 2024

Abstract
Perovskite-like oxides present huge chemical variability and a wide range of applications as catalysts for oxidation reactions. The interaction of several small gas molecules with the surface of $LaCoO_3$ and $LaMnO_3$ perovskite-like oxides was studied by Near Ambient Pressure X-ray photoelectron spectroscopy (NAP-XPS) and CO Temperature Programmed Desorption (CO-TPD). Surface chemical changes such as the $O_{surf}/O_{lattice}$ and cation B oxidation state ratios were analyzed as a function of temperature (400 K, 450 K, 500 K, 550 K, and 650 K) under different gas atmospheres like Ar, CO, H_2, and O_2. It was found that there was a partial surface reduction when H_2 and CO were used in the reaction, and therefore, the cation B oxidation state (Mn^{4+}/Mn^{3+} and Co^{3+}/Co^{2+}) ratio decreased. Under the CO stream, carbonate species were formed, presenting a C1s signal between 284.5 eV and 287 eV. The CO_2 evolution during the reaction at temperatures greater than 500 K was associated with CO activation over or near to surface oxygen species. A Mars-van Krevelen mechanism was proposed for the process, finding significant differences between $LaCoO_3$ and $LaMnO_3$ perovskite-like solid catalysts behavior.

Keywords CO oxidation · Vacancy effect · B cation effect · NAP-XPS

1 Introduction

Carbon monoxide oxidation and selective oxidation (SELOX) has been widely used as a model reaction for catalytic systems and is frequently used for oxide catalysts that present oxygen mobility and active metals [1]. One of the most common interests is understanding how oxygen mobility affects surface-molecule interaction. Computational and experimental works have given some indication of these effects. Nevertheless, it is challenging to understand how the chemical environment of these systems changes without an XPS analysis that determines the average oxidation state of surface atoms [1, 2].

Several studies have been reported under UHV (ultra-high vacuum) conditions. Here, the main limitation for interpreting the obtained results is that the solids are under a quite low pressure in the analysis chamber ($\sim 1 \times 10^{-10}$ mbar). This limitation involves a challenge in comparing UHV-XPS and experimental results with information obtained at atmospheric pressure because the experimental conditions are significantly different, which leads to non-equivalent thermodynamic systems [3–5].

NAP-XPS (*Near Ambient Pressure X-ray Photoelectron Spectroscopy*) was developed to obtain a surface analysis that is more realistic in comparison to experiments carried out at atmospheric pressure [4–7]. The metal surface role in the adsorption process is one of the trending topics in catalysis [8–12]. Studying the chemical environment and understanding possible surface-molecule interactions in heterogeneous catalysis are of great interest. Therefore, the technological development of the NAP-XPS technique has been classified as one of the great tools for understanding surface chemistry and the possible chemical changes on a surface when it is interacting with different molecules and at different temperatures [1, 13], which involves *in-situ* or *in-operando* methodologies.

✉ Juan Tapia-P.
juan.tapia@udea.edu.co

[1] Química de Recursos Energéticos y Medio Ambiente, Instituto de Química, Facultad de Ciencias Exactas y Naturales, Universidad de Antioquia UdeA, Calle 70 No. 52-21, Medellín, Colombia

[2] Center for Materials Research, Justus-Liebig University, Heinrich-Buff-Ring 17, 35392 Giessen, Germany

[3] Institute of Physical Chemistry, Justus-Liebig University, Heinrich-Buff-Ring 17, 35392 Giessen, Germany

[4] GeoRessources, Université de Lorraine, CNRS, 54000 Nancy, France

Published online: 17 August 2024

Many scientific reports analyze catalyst surfaces based on well-structured catalytic systems using mostly noble metals as Pt (110) [14], Pd (111) [15], or bimetallic systems like CoPt [16], and PtTi [17], as well as Cu based systems Cu (111) [18]. Also, many studies are based on Au nanoparticles supported on different high surface area oxides [19–21]. However, the world trend is to look for new and cheap alternatives that allow the development of catalytic systems based on transition metals. In this sense, few publications study systems that have less defined or polycrystalline structures which make the system more complicated [22–25]. In this regard, cobalt as a metal oxide is probably the most studied system in terms of *in-situ* reactions into NAP cells. Some works based on preferential oxidation (PROX) have been presented to study the role of cobalt species and the role of palladium doping and its possible mechanisms [26–28].

In addition, recent studies, using transition metal oxides (simple or mixed) such as perovskite-like solids that can be used as a catalytic system, or in solid oxide fuel cell (SOFC) applications, electrochemistry systems, or oxidation catalyst due to oxygen mobility and surface defects. However, the study of temperature and gas–like effects over the surface on the CO oxidation reaction is not well studied. In this work, the different surface changes that undergo perovskite-like oxides, specifically $LaCoO_3$ and $LaMnO_3$, exposed to different kinds of gas molecules (reducing, oxidizing, and inert gas: H_2, CO, O_2, and Ar) were investigated, as well as the modified mechanism of Mars-van Krevelen (Mv-K).

2 Methodology

2.1 Catalyst Preparation

$LaBO_3$ (B: Mn or Co) perovskite-like oxides were synthesized by self-combustion methodology [29]. The ignition promoter, glycine ($H_2NCH_2CO_2H$, PanReac), was added to an aqueous metal nitrate solution at the required stoichiometric amount to get a NO_3^-/NH_2 ratio of 1. $La(NO_3)_3 \bullet 6H_2O$, $Mn(NO_3)_3 \bullet 4H_2O$, and $Co(NO_3) \bullet H_2O$ (PanReac) were used as metal precursors. The solution was slowly evaporated under magnetic stirring at about 373 K until a gel-like appearance was obtained. The gel was heated up to around 523 K, a temperature at which the ignition reaction occurs, producing a powdered precursor containing carbon residues. Therefore, all solids were calcined in static air for 8 h, at 873 K and using a heating rate of 10 K•min^{-1}, to promote the solid organization and to form a perovskite-like structure. LC and LM are used to represent $LaCoO_3$ and $LaMnO_3$ samples, respectively.

2.2 CO Temperature Programmed Desorption (CO-TPD)

CO-TPD experiments were performed with a Chemisorption AutoChem 2920 Micromeritics®, using a thermal conductivity detector (TCD). Around 100 mg of the oxide sample (grain size between 74 µm and 149 µm) was inserted into a U quartz reactor and pretreated at 873 K for 15 min under a 10% O_2/He (in volumetric fraction) gas flow. Then, the sample was stabilized at 323 K and pulses of 5% CO (in volumetric fraction) in He balance were sent, using a 0.6 cm^3 fixed volume loop, until reaching the sample reached saturation as indicated by a constant TCD signal. After that, the gas was switched to pure argon (30 mLmin^{-1}) and the temperature increased to 873 K with a heating rate of 10 K•min^{-1}. The equipment was coupled to a quadrupole mass spectrometer (Pfeiffer QMS OmniStar 300c equipment). The intensity of M/Z signals: 18, 28, 32, and 44, corresponding to: H_2O^+, CO^+, O_2^+, and CO_2^+, respectively, were monitored continuously while raising the temperature up to 873 K.

Temperature-programmed reduction (H_2-TPR) and temperature-programmed desorption (O_2-TPD) experiments were performed with the previous equipment. Around 100 mg of the oxide sample (with a grain size between 74 µm and 149 µm) was inserted into a U quartz reactor and pretreated at CT for 15 min under a gas flow of 10% O_2/Ar (in volumetric fraction). H_2-TPR experiments were performed with a 5% H_2/Ar (30 mL•min^{-1}) and the temperature reached 873 K at a heating rate of 10 K•min^{-1}. O_2-TPD experiments were performed under pure argon flow at 30 mL•min^{-1} and the temperature reached 873 K at heating rate of 10 K•min^{-1}.

2.3 X-ray Photoelectron Spectroscopy – near Ambient Pressure (XPS-NAP)

XPS analysis was performed on a Specs equipment with PHOIBOS 1501D-DLD analyzer, with a monochromatized Al-Kα (1486.7 eV, 13 kV, 100 W) source and passing energy of 1 30 eV. The binding energy (BE) was corrected using *C1s* of adventitious carbon, with a binding energy of 284.8 eV, as a reference. XPS spectra were decomposed by a curve fitting after the Shirley-type background subtraction using CasaXPS software [30].

The *in-situ* cell was operated at 1 mbar that is fixed using a gas flow around of 0.5 mL•min^{-1} and the temperature was increased from 400 to 650 K, while the signals of *Mn2p, Co2p, O1s y C1s* were followed. The pressure increased as a function of temperature up to a maximum value of 2 mbar.

Ar, O_2, CO, H_2, CO/O_2 were used as inert, oxidant, and reductive atmospheres (UHP, 99.999% purity) respectively.

These gases are used to analyze the different surface changes at *in-situ* conditions simulating CO oxidation reaction environments. A sample powder was used for all experiments, and the gases were dosed in the previously mentioned order.

The gaseous products were followed with a mass spectrometer (Pfeiffer QMS) to analyze possible reaction products.

3 Results

3.1 Adsorption–desorption Analysis by CO and O_2 TPD

The temperature-programmed analysis for $LaMnO_3$ and $LaCoO_3$ is shown in Fig. 1, including CO oxidation (with and without hydrogen), H_2-TPR, and O_2-TPD. Cobalt-based catalyst in Fig. 1 shown the reducibility can help enhance the reactivity of the oxidation reaction as seen in the plot given the reduction of 50 K at T_{50} in oxidation temperature when comparing the reaction with and without hydrogen, due to probably to water production [31]. However, for the manganese-based catalyst, this type of effect does not seem to affect the catalytic performance for oxidation reactions, finding the same profile in both reactions. It is possible to appreciate how the oxygen desorption profiles are directly related to CO oxidation profiles in both cases, giving a clear idea of the effect that labile oxygens have on the surface reactivity, as has been reported by other authors [22, 32, 33].

The catalytic cycle effect as a test of REDOX properties for the used material is shown in Fig. 2. Four CO adsorption–desorption cycles were compared with O_2-TPD, and one desorption where all the surface labile oxygen was desorbed (reduced surface). It can be observed that the solid reactivity indirectly measured by O_2-TPD is well correlated with the adsorption–desorption process, this is because it has a similar desorption profile, and the changes in each cycle are not significant. Additionally, the CO adsorbed at 323 K is desorbed in all cases as CO_2, which means that there is a reaction taking place with the surface oxygen from the solid, as has been previously reported [34]. It should be noted that the processes at this level are evidenced in the replication of the desorption profiles as a function of the number of cycles, and there is a slight variation which is probably due to partial poisoning of active sites by carbonate species formation or strongly adsorbed species [35, 36].

However, the catalytic activity is almost the same in the four analyzed cycles. On the other hand, Table 1 shows the quantification of CO adsorbed using CO pulses, providing an idea of the adsorption-reaction capacity of the solid. It is observed that the solid loses adsorption capacity when increasing the number of cycles; this result is expected

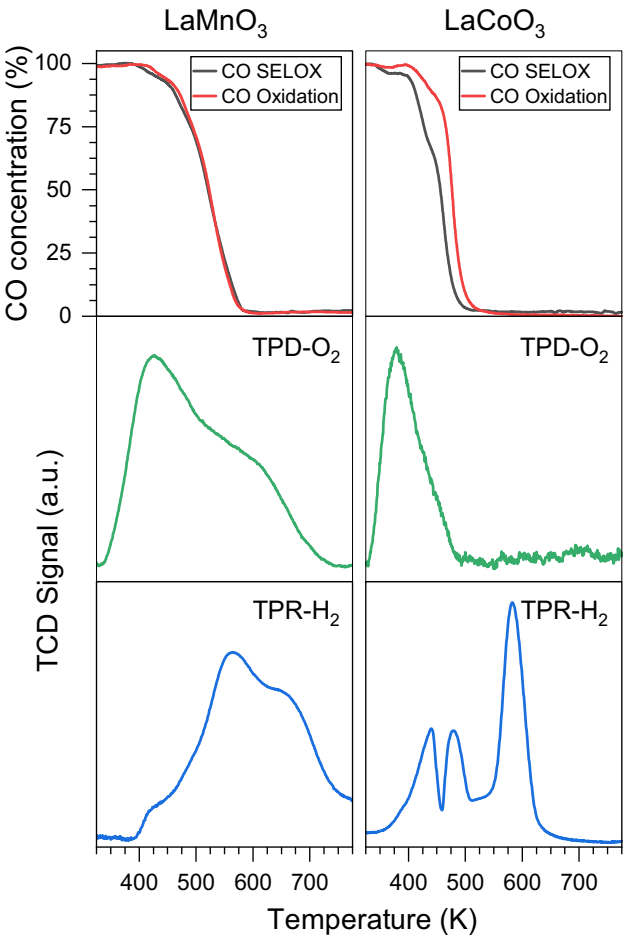

Fig. 1 CO oxidation reaction profiles (with and without H_2), O_2TPD, and H_2-TPR for $LaMnO_3$ and $LaCoO_3$

because the solid surface undergoes a transformation or partial poisoning until stabilized. In addition, carbonate formation could poison some active sites. In similar experiments, Sierra et al. [37] used methane pulses in a methane reforming reaction model. However, they did not quantify the methane mole adsorbed per cycle since it hints at solid poisoning. Desorption profiles showed the evolution of not only carbon dioxide but also water and oxygen. Figure 3 shows the different species that desorb from the solid pretreated with a mixture of 10% O_2 (in volumetric fraction) in argon at 323 K. Therefore, CO_2, CO, and O_2 desorption would be expected. However, it is observed that the water signal has a more significant contribution than the other desorption signals. This is probably taking place because the employed gases seem to have traces of water that are adsorbed on the solid during the pretreatment process, and the water mass spectrometer response is higher than for the other molecules. At working temperature, any other type of reaction is ruled out.

Additionally, it is well known that La-based compounds are highly basic and react strongly with water and carbon dioxide to form hydroxides, carbonates, and oxi-carbonates [38, 39].

The CO-TPD-Red in Fig. 2. shows the desorption profile after CO saturation over an oxygen-free surface. The experiment does not show desorption of any species (CO/CO_2) and this result is related to the absence of labile oxygen. Additionally, the CO adsorbed can be either strongly molecular or form highly stable species like carbonate or carbide. It can also be assumed that strong CO adsorption means that this molecule adsorption is easier over a clean surface free of labile oxygen than over an oxidized surface. The active sites created by the oxygen desorption can be used for the adsorption of CO, and oxygen. On the other hand, if the CO absorbed does not find a labile oxygen, or that has been adsorbed in the catalytic process, it is strongly chemisorbed. Therefore, it would form a very stable species, requiring high temperatures to be desorbed.

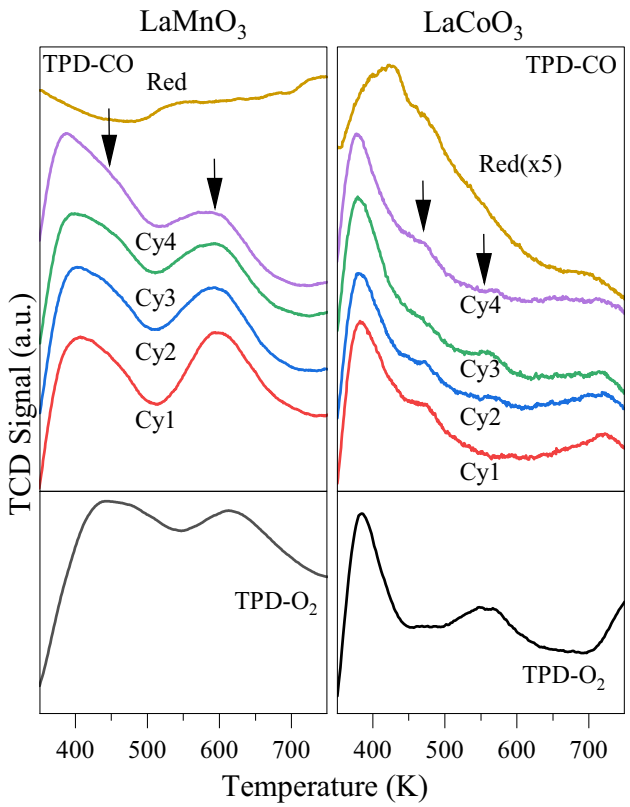

Fig. 2 Temperature programmed desorption of oxygen and CO (O_2-TPD, CO-TPD) for $LaMnO_3$ and $LaCoO_3$. The cycles consist of several steps: *Step 1*: heat up to 873 K in 10% O_2/He. Step 2: Cool down at room temperature and cleaning with helium. *Step 3*: CO saturation at room temperature using 5% CO/He. *Step 4*. Temperature programmed of desorption up to 873 K. This entire process is repeated four times using the same sample. Step 1 was done in He for CO-TPD-Red to desorb all the labile oxygen, red (×5) indicates a signal magnification. Arrows show the changes in profile

Table 1 Amount of CO adsorbed in micro-mol per gram of catalyst, quantifying the injected pulses (5% CO/He). The deviation of the results does not exceed 5%

	$LaMnO_3$ ($\mu mol \bullet g^{-1}$)	$LaCoO_3$ ($\mu mol \bullet g^{-1}$)
Cycle 1	243.4	213.4
Cycle 2	158.53	175.4
Cycle 3	128.10	143.6
Cycle 4	127.7	136.6
Pulse red*	288.4	287.5

*: Experiment carried out with the clean oxygen labile surface

3.2 NAP-XPS Analysis

The NAP-XPS experiments were carried out following the next specific order using the same sample for all experiments in the presence of Ar, O_2, H_2, CO, and $CO + O_2$ (5 mbar of dynamic pressure in the in-situ cell). For each gas, two hours were expended to ensure that the chamber is filled and purged. The pressure in the chamber is 0.5 mbar and it is purged with the next analysis gas until the signal from the previous gas cannot be seen in the mass spectrometer. In addition, quick runs are carried out during the warm-ups to see if there is any change in this process. The temperature was increased from 400 to 650 K and every 50 Kelvin the metal and oxygen XPS spectra were taken to analyze the surface changes.

Changes in oxygen ratio ($O_{Lattice}/O_{Surf}$) and cation B oxidation state ratio (Co^{3+}/Co^{2+}, Mn^{4+}/Mn^{3+}) as a function of temperature for several gas atmospheres are shown in Fig. 4. These results clearly show that the temperature and the gas nature change these atomic ratios on the surface materials. The gases can be separated into three types depending on their chemical nature: H_2 and CO as reducing agents; O_2 as oxidizing; and argon as inert.

The reducing agent gases would displace surface oxygen, inducing a partial reduction reflected in the decrease of Co^{3+}/Co^{2+} and Mn^{4+}/Mn^{3+} atomic ratios, as shown in Fig. 4. As expected, the opposite result happens with oxygen. Argon, being an inert gas, may not have any effect. Nevertheless, the thermal impact here is significant. It reduces partial surface by displacing the labile oxygen from the surface to the gas phase, creating oxygen vacancies.

The expected behavior for the LC sample was observed, which involves a reduction in a rich argon atmosphere but an oxidation in an oxygen atmosphere. However, a partial reduction is observed for the LM sample when exposed to an atmosphere of argon or oxygen. It is also shown that oxygen adsorbed or alfa-oxygen on the surface can be more easily desorbed than the possible adsorption of gas molecules. Therefore, the thermal effect seems to be more important than the nature of the gas atmosphere. The $CO + O_2$ mixture

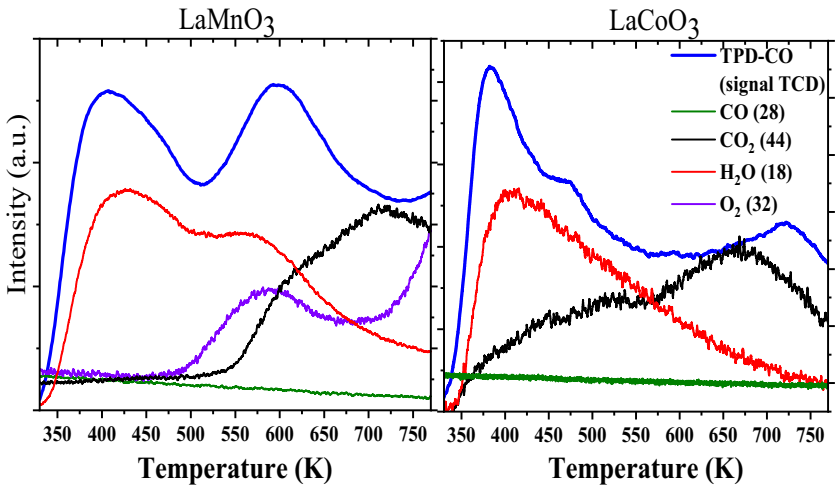

Fig. 3 CO-TPD plot coupled to mass spectrometer. Following mass signals related to CO oxidation

analysis shows that changes in metal and oxygen atomic ratios are not significant regarding the temperature.

In this system, CO_2 as a reaction product was monitored by mass spectrometry following the signal M/Z = 44. Here, it was observed how this signal increased with rising temperature (Fig. 5). Previous studies using cobalt have reported results similar to those in this study [40, 41].

The following equations outline how the catalyst acts, depending on the cation B (Mn or Co), one rich in surface oxygen and another rich in vacancies. This causes changes on the surface and in how they interact with the test molecules.

$$Mn - O - Mn \xrightarrow{\cdots CO_{(g)}\cdots} CO - Mn - O - Mn \rightarrow CO_{2(g)} + Mn - [V_O] - Mn \quad (1)$$

$$C_O - [V_O] - C_O \xrightarrow{O_{2(g)}} C_O - \boldsymbol{O} - C_O - \boldsymbol{O} \xrightarrow{2CO_{(g)}} 2\boldsymbol{CO}_{2(g)} + C_O - [V_O] - C_O \quad (2)$$

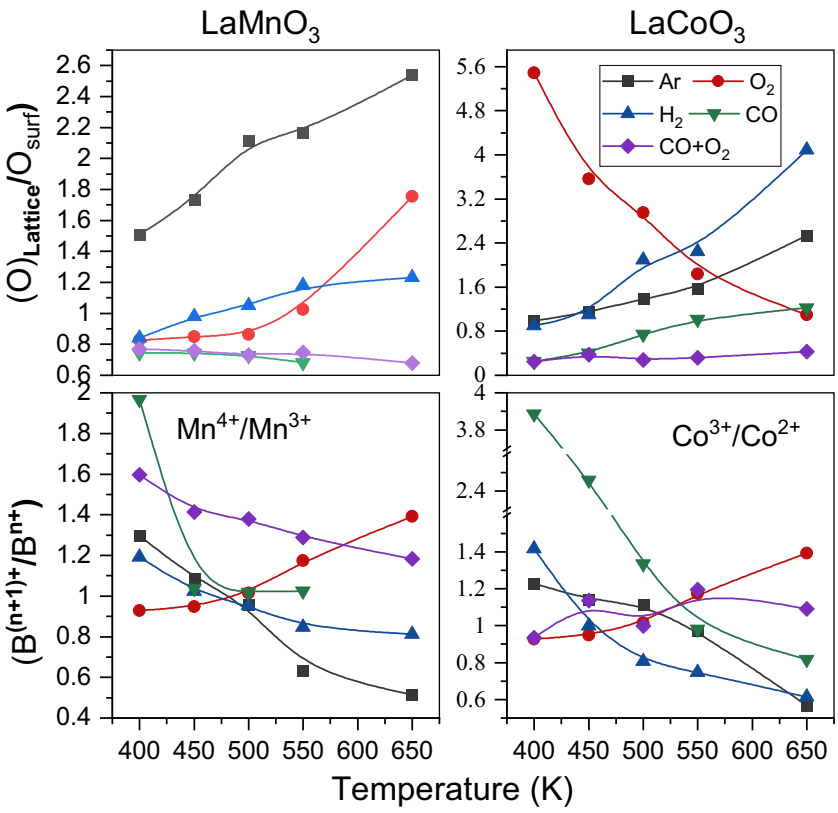

Fig. 4 Atomic ratio for oxygen ($O_{Lattice}/O_{Surf}$) and cation B (Co^{3+}/Co^{2+}, Mn^{4+}/Mn^{3+}) calculated from all NAP-XPS experiments with several gases and temperatures

Figure 5 shows that the changes in carbon dioxide formation are not significant concerning metal or temperature, this is because the experiments are carried out at a maximum of 5 mbar, which implies few molecules in the in-situ cell. Therefore, the gas output does not represent the total moles that reacted.

The C1s spectra for the experiments performed with a mixture of $CO + O_2$ at different temperatures are shown in Fig. 6. When the experiment is set up in CO atmosphere, CO adsorbed and carbon 1 s signal emerges in the solid surface between 284.5 eV and 286 eV. These signals are formed at 400 K for the LC sample but tend to disappear when temperature increases. On the other hand, the observed trend for the LM sample is the opposite to the LC sample. Additionally for LM sample, the formation of the CO adsorbed C1s signal is obtained from 500 K and progressively increases up to 650 K. It is noteworthy that at temperatures below 500 K it is not possible to see this signal nor at room temperature. This result gives an idea of a change in the mechanism that may occur in the oxidation reaction. Therefore, it can be deduced that the LC perovskite-like oxide is more active than the LM sample since it can adsorb CO at low temperatures and regenerates its surface at high temperatures (i.e. 650 K). However, at high temperatures, the adsorption–desorption processes are so fast that the C1s from CO-ads cannot be detected.

In all the experiments, the C1s signal-to-noise ratio is high compared to the other followed signals due to the low pressure and CO concentration in the chamber, which is not surprising since similar reports have been reported in other studies [40, 41]. Although, in these reports, it was possible to see the formation of C1s carbonates after the surface was cleaned from the C1s adventitious, which is conventionally intense.

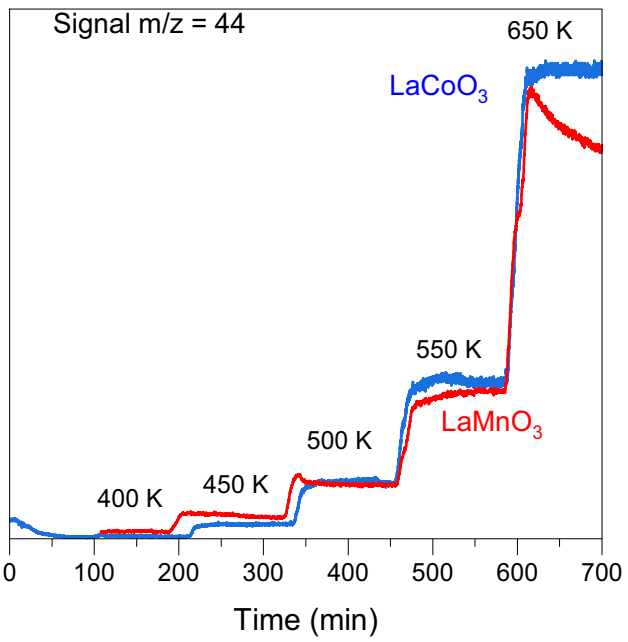

Fig. 5 CO_2 signal (M/Z = 44) followed by mass spectrometry at the exit of *in-situ* cell on the NAP-XPS equipment

It should be noted that these species are highly stable in other systems, generally basic, but for this study, they appear to be labile species that may or may not have an influence on reactivity, and that will depend on the temperature at which the reaction is taking place. These species are spectators since they do not participate in the reaction until a critical temperature is reached where they can be desorbed as CO_2, leaving oxygen on the surface [42].

3.3 CO Oxidation on Perovskite-like Oxide Surfaces

The proposed mechanisms are shown in Fig. 7, Fig. 8, and Fig. 9. where the possible steps involved in the reaction are outlined from two points of view based on the modified mechanism of Mar Van Krevelen (MVK) [42], showing probable mechanisms for these reactions based on the above information.

The oxidation reaction cycle is shown in Fig. 7, starting from a clean surface that adsorbs CO, and the subsequent CO_2 formation. From this step, there are two possible options, the desorption of the CO_2 molecule, as seen in the diagram, until the original surface is recovered, or the reaction with another oxygen to form a spectator carbonate species, which has been reported as a very stable species [43]. However, as seen in Fig. 6, this behavior changes for both materials depending on the temperature at which the reaction occurs. The MVK mechanism does not consider the carbonate species formed in the reaction, which modifies the reaction redox cycle, regardless of whether it is an active species or only a spectator.

On the other hand, in Fig. 8, the catalyst surface's redox cycles are shown schematically, as they are in contact with different types of atmospheres (gas supply). Depending on the temperature of the non-reactive gas, the vacancy formation and the partial reduction of the surface are argued, which can then be rebuilt by adding oxygen. Moreover, a substantial reduction compared to Ar can take place, using CO or H_2 to form CO_2 or water, respectively, with the formation of oxygen vacancies by the abstraction of oxygen from the surface, as shown in the CO-TPD and O_2-TPD results. The ability of a solid to indefinitely complete these REDOX cycles makes it possible to measure its oxygen mobility capacity and catalytic efficiency [22, 44].

The reaction schemes adjusted to the perovskite-like catalysts are shown in Fig. 9. In the case of the LC solid, when the surface is under Ar conditions, the density of vacancies increases, which promotes a partially reduced surface ($LaCo^{3+,2+}O_{3-\delta}$). Whereby, the first step in the mechanism would be the adsorption of O_2 to fill up the

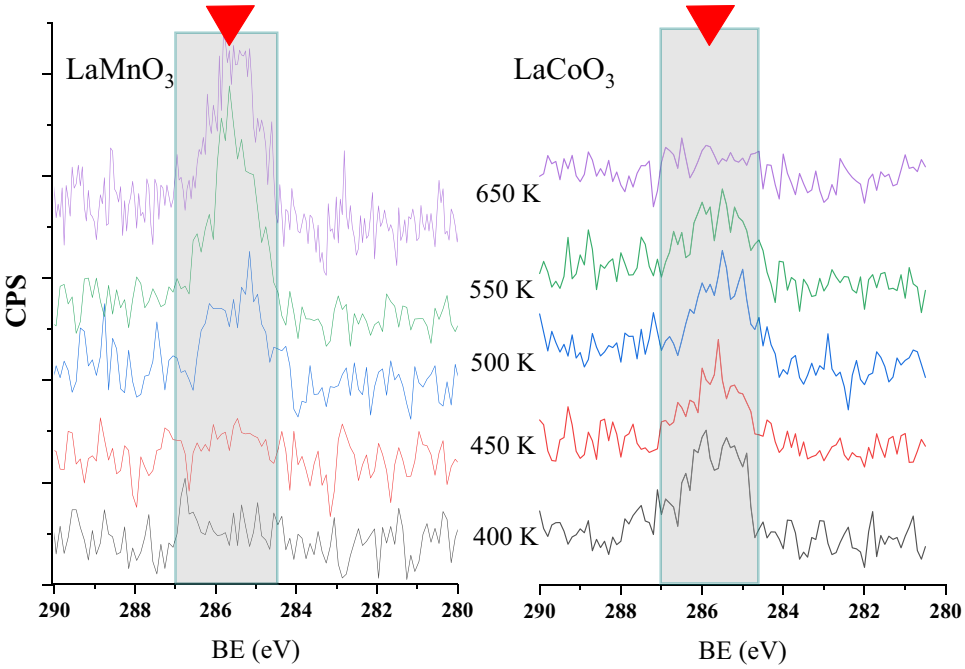

Fig. 6 *In-situ* NAP-XPS C1s spectra for LC and LM under $CO+O_2$ mixture at 5 mbar and continuous flow at different temperatures. RT is the C1s signal after oxygen pretreatment, at this stage there is no signal of carbon and the surface is pristine. The values for signal noise ratio (SNR) for LC and LM for the most intense peak is 8.5 and 11.3 respectively

vacancies, which improves the activation of the oxygen molecule. On the other hand, the LM solid, which is oxophilic, has many adsorbed oxygens, as shown in Fig. 1, and has an over-oxidized surface ($LaMn^{3+,4+}O_{3+\delta}$). Therefore, in the first step of the reaction process, two simultaneous steps are taken: desorption of weakly adsorbed O_2 and adsorption of CO. After that, the process follows the same oxidation steps shown in Fig. 7.

In addition, the formation of vacancies happens as the desorption of O atoms as molecular oxygen from the surface takes place, which implies a reduction of the Mn^{4+} to Mn^{3+} ratio, However, this is not evident in the XPS spectra, and there is another option where there are species like pairs V_O-V_{Mn}, which allow observing vacancies. This is important since vacancies are thermodynamically expected on a perovskite-like surface.

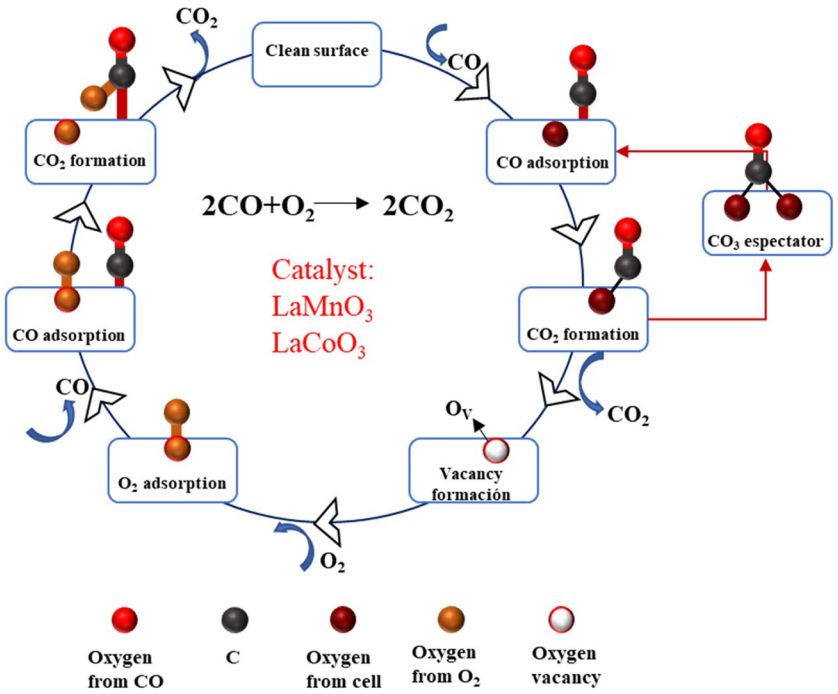

Fig. 7 The cyclic reaction mechanism based on the Mars-van Krevelen model shows carbonate species' impact

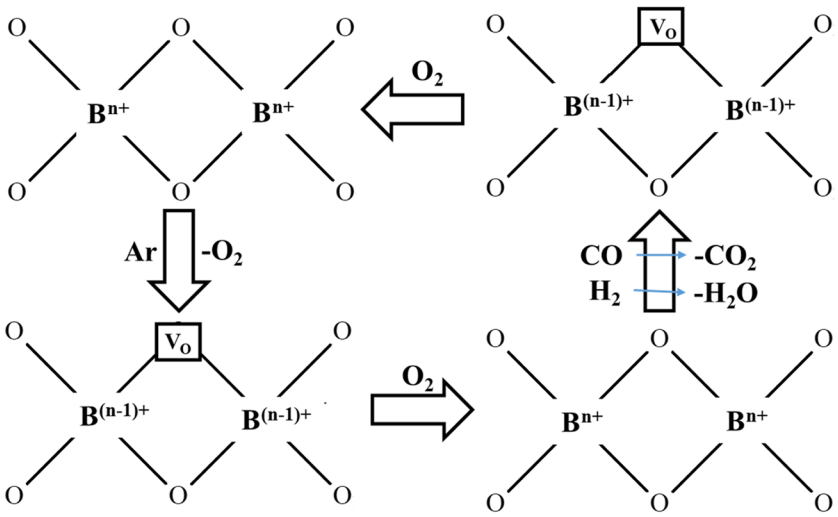

Fig. 8 Simplified redox cyclic scheme of perovskite-like $La(Mn,Co)O_{3\pm\delta}$ surface where the superscript "n" is the metal charge and can vary depending on the gas character (reductive, oxidative, or inert), pressure, and temperature

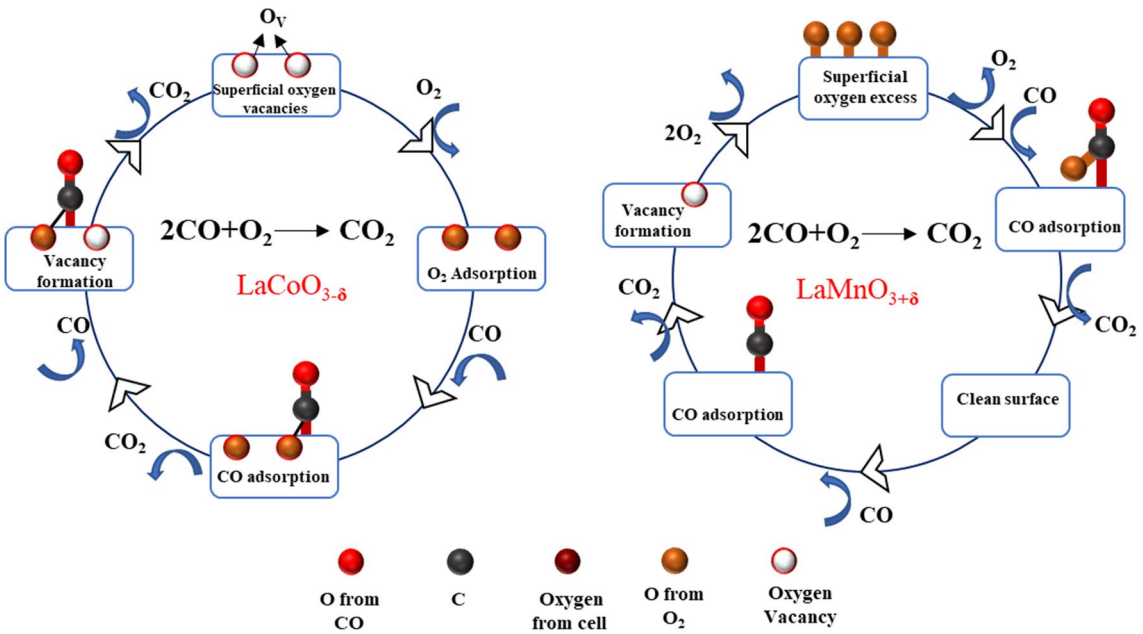

Fig. 9 CO oxidation cyclic reaction mechanism based on the Mars-van Krevelen model adapted to $LaMnO_{3+\delta}$ and $LaCoO_{3-\delta}$ perovskite-like oxides

4 Conclusions

It was possible to evidence the redox nature at the macro level, with the CO adsorption experiments (CO-TPD), and to observe small variations in the desorption profiles, where the presence of CO_2 is detected as a reaction product when CO reacts with labile oxygen from the surface.

The *in-situ* NAP-XPS technique allows to analyze the redox surface changes caused by the interaction with different kinds of gas molecules. The gas nature and the temperature play an important role in the electronic changes caused by the interaction of reactive molecules on the catalyst surface. CO and H_2 have reducing effects while oxygen oxidize the surface and Ar, being inert, allows a surface reduction due to a thermal effect. All these analyses allow the understanding of these oxides' redox nature, illustrating the structure's adaptability, as well as its use and efficiency in different reactions. On the other hand, the presence of adsorbed carbon species on the surface formed by the decomposition of CO was observed, at low temperatures for the LC sample and at high temperatures for the LM sample, which suggests different reaction mechanisms for both surfaces.

Supplementary Information The online version contains supplementary material available at https://doi.org/10.1007/s10562-024-04778-9.

Funding Open Access funding provided by Colombia Consortium.

Declarations

Conflict of Interest The authors declare no competing financial interest.

References

1. Royer S, Duprez D (2011) Catalytic Oxidation of Carbon Monoxide over Transition Metal Oxides. ChemCatChem 3(1):24–65
2. Yang J, Hu S, Fang Y, Hoang S, Li L, Yang W et al (2019) Oxygen vacancy promoted o2 activation over perovskite oxide for low-temperature co oxidation. ACS Catal 9(11):9751–9763
3. Venezia AM (2003) X-ray photoelectron spectroscopy (XPS) for catalysts characterization. Catal Today 77(4):359–370
4. Turner NH, Schreifels JA (2000) Surface analysis: X-ray photoelectron spectroscopy and Auger electron spectroscopy. Anal Chem 72(12):99–110
5. Salmeron M, Schlögl R (2008) Ambient pressure photoelectron spectroscopy: A new tool for surface science and nanotechnology. Surf Sci Rep 63(4):169–199
6. Nguyen L, Tao FF, Tang Y, Dou J, Bao XJ (2019) Understanding Catalyst Surfaces during Catalysis through Near Ambient Pressure X-ray Photoelectron Spectroscopy. Chem Rev 119(12):6822–6905
7. Zhong L, Chen D, Zafeiratos S (2019) A mini review of in situ near-ambient pressure XPS studies on non-noble, late transition metal catalysts. Catal Sci Technol 9(15):3851–3867
8. Ganduglia-Pirovano MV, Hofmann A, Sauer J (2007) Oxygen vacancies in transition metal and rare earth oxides: Current state of understanding and remaining challenges. Surf Sci Rep 62(6):219–270
9. Liu D, Wang C, Yu Y, Zhao BH, Wang W, Du Y et al (2019) Understanding the Nature of Ammonia Treatment to Synthesize Oxygen Vacancy-Enriched Transition Metal Oxides. Chem. 5(2):376–89. https://doi.org/10.1016/j.chempr.2018.11.001
10. Li X, Ma J, Yang L, He G, Zhang C, Zhang R et al (2018) Oxygen Vacancies Induced by Transition Metal Doping in γ-MnO 2 for Highly Efficient Ozone Decomposition. Environ Sci Technol 52(21):12685–12696
11. Xu W, Lyu F, Bai Y, Gao A, Feng J, Cai Z et al (2018) Porous cobalt oxide nanoplates enriched with oxygen vacancies for oxygen evolution reaction. Nano Energy. 43:110–6. https://doi.org/10.1016/j.nanoen.2017.11.022
12. Royer S, Duprez D, Kaliaguine S (2006) Oxygen mobility in LaCoO3 perovskites. Catal Today 112(1–4):99–102
13. Nenning A, Opitz AK, Rameshan C, Rameshan R, Blume R, Hävecker M et al (2016) Ambient pressure XPS study of mixed conducting perovskite-type SOFC cathode and anode materials under well-defined electrochemical polarization. J Phys Chem C 120(3):1461–1471
14. Butcher DR, Grass ME, Zeng Z, Aksoy F, Bluhm H, Li WX et al (2011) In situ oxidation study of Pt(110) and its interaction with CO. J Am Chem Soc 133(50):20319–20325
15. Toyoshima R, Yoshida M, Monya Y, Kousa Y, Suzuki K, Abe H et al (2012) In situ ambient pressure XPS study of CO oxidation reaction on Pd(111) surfaces. J Phys Chem C 116(35):18691–18697
16. Zheng F, Alayoglu S, Pushkarev VV, Beaumont SK, Specht C, Aksoy F et al (2012) In situ study of oxidation states and structure of 4 nm CoPt bimetallic nanoparticles during CO oxidation using X-ray spectroscopies in comparison with reaction turnover frequency. Catal Today. 182(1):54–9. https://doi.org/10.1016/j.cattod.2011.10.009
17. Jeong C, Yun H, Lee H, Muller S, Lee J, Mun BS (2016) Performance test of new near-ambient-pressure XPS at Korean Basic Science Institute and its application to CO oxidation study on Pt3Ti polycrystalline surface. Curr Appl Phys 16(1):73–8. https://doi.org/10.1016/j.cap.2015.10.010
18. Eren B, Heine C, Bluhm H, Somorjai GA, Salmeron M (2015) Catalyst Chemical State during CO Oxidation Reaction on Cu(111) Studied with Ambient-Pressure X-ray Photoelectron Spectroscopy and Near Edge X-ray Adsorption Fine Structure Spectroscopy. J Am Chem Soc 137(34):11186–11190
19. Jiang P, Porsgaard S, Borondics F, Kober M, Caballero A, Bluhm H et al (2010) Room-temperature reaction of oxygen with gold: An in situ ambient-pressure x-ray photoelectron spectroscopy investigation. J Am Chem Soc 132(9):2858–2859
20. Dumbuya K, Cabailh G, Lazzari R, Jupille J, Ringel L, Pistor M et al (2012) Evidence for an active oxygen species on Au/TiO 2(1 1 0) model catalysts during investigation with in situ X-ray photoelectron spectroscopy. Catal Today. 181(1):20–5. https://doi.org/10.1016/j.cattod.2011.09.035
21. Herranz T, Deng X, Cabot A, Alivisatos P, Liu Z, Soler-Illia G et al (2009) Reactivity of Au nanoparticles supported over SiO2 and TiO2 studied by ambient pressure photoelectron spectroscopy. Catal Today 143(1–2):158–166
22. Royer S, Duprez D, Can F, Courtois X, Batiot-Dupeyrat C, Laassiri S et al (2014) Perovskites as substitutes of noble metals for heterogeneous catalysis: Dream or reality. Chem Rev 114(20):10292–10368
23. Tarjomannejad A, Niaei A, Farzi A, Salari D, Zonouz PR (2016) Catalytic Oxidation of CO Over LaMn1−xBxO3 (B = Cu, Fe) Perovskite-type Oxides. Catal Letters 146(8):1544–1551
24. Chagas CA, Magalhães RNSH, Schmal M (2021) The LaCo1−xVxO3 Catalyst for CO Oxidation in Rich H2 Stream. Catal Lett 151(2):409–21. https://doi.org/10.1007/s10562-020-03303-y
25. Huang X, Yang N, Li X, Pan H, Song X, Chang Y (2022) La0.8Sr0.2MnO3 Perovskite Catalysts Prepared by Different Methods for CO Oxidation. Catal Lett 152(12):3843–52. https://doi.org/10.1007/s10562-022-03921-8
26. Xu H, Fu Q, Guo X, Bao X (2012) Architecture of Pt-Co Bimetallic Catalysts for Catalytic CO Oxidation. ChemCatChem 4(10):1645–1652
27. Liu K, Wang A, Zhang T (2012) Recent advances in preferential oxidation of co reaction over platinum group metal catalysts. ACS Catal 2(6):1165–1178
28. Wang C, Li B, Lin H, Yuan Y (2012) Carbon nanotube-supported Pt-Co bimetallic catalysts for preferential oxidation of CO in a H 2-rich stream with CO 2 and H 2O vapor. J Power Sources. 202:200–8. https://doi.org/10.1016/j.jpowsour.2011.11.044
29. Chick LA, Pederson LR, Maupin GD, Bates JL, Thomas LE, Exarhos GJ (1990) Glycine-nitrate combustion synthesis of oxide ceramic powders. Mater Lett 10(1–2):6–12

30. Fairley N, Fernandez V, Richard-Plouet M, Guillot-Deudon C, Walton J, Smith E et al (2021) Systematic and collaborative approach to problem solving using X-ray photoelectron spectroscopy. Appl Surf Sci Adv 5(100112):1–9. https://doi.org/10.1016/j.apsadv.2021.100112
31. Shen K, Gorte RJ, Vohs JM (2023) H_2O promotion of CO oxidation on oxidized Pt/CeFeOx. Catal Lett 154:2414–2421. https://doi.org/10.1007/s10562-023-04480-2
32. Tapia-P J, Gallego J, Espinal JF (2021) Calcination Temperature Effect in Catalyst Reactivity for the CO SELOX Reaction Using Perovskite-like LaBO3 (B: Mn, Fe Co, Ni) Oxides. Catal Lett 151(12):3690–703. https://doi.org/10.1007/s10562-021-03601-z
33. Tapia-P J, Cao Y, Gallego J, Osorio-Guillén JM, Morgan D, Espinal JF (2022) CO Oxidation catalytic effects of intrinsic surface defects in rhombohedral $LaMnO_3$. ChemPhysChem 23(11):1–8. https://doi.org/10.1002/cphc.202200152
34. Zhu J, Zhao Z, Xiao D, Li J, Yang X, Wu Y (2005) CO oxidation, NO decomposition, and NO + CO reduction over perovskite-like oxides La2CuO4 and La2-xSrxCuO 4: An MS-TPD study. Ind Eng Chem Res 44(12):4227–4233
35. Hwang J, Rao RR, Katayama Y, Lee D, Wang XR, Crumlin E et al (2018) CO2 Reactivity on Cobalt-Based Perovskites. J Phys Chem C. 122(35):20391–401. https://doi.org/10.1021/acs.jpcc.8b06104
36. González-Varela D, Araiza DG, Díaz G, Pfeiffer H (2022) $LaNiO_3$ perovskite synthesis through the EDTA–citrate complexing method and its application to CO oxidation. Catalysts 12(1):1–17. https://doi.org/10.3390/catal12010057
37. Sierra G, Batiot-Dupeyrat C, Mondragón F (2010) Methane partial oxidation by the lattice oxygen of the lanio3δ perovskite. a pulse study. Dyna. 77(163):141–50
38. Sato S, Takahashi R, Kobune M, Gotoh H (2009) Basic properties of rare earth oxides. Appl Catal A Gen 356(1):57–63 (https://www.sciencedirect.com/science/article/pii/S0926860X08007813)
39. Branco JB, Brito PE, Ferreira AC (2020) Methanation of CO2 over nickel-lanthanide bimetallic oxides supported on silica. Chem Eng J 380:122465 (https://www.sciencedirect.com/science/article/pii/S1385894719318686)
40. Lukashuk L, Föttinger K, Kolar E, Rameshan C, Teschner D, Hävecker M et al (2016) Operando XAS and NAP-XPS studies of preferential CO oxidation on Co3O4 and CeO2-Co3O4 catalysts. J Catal 344:1–15. https://doi.org/10.1016/j.jcat.2016.09.002
41. Lukashuk L, Yigit N, Kolar E, Teschner D, Rupprechter G (2018) Operando Insights into CO Oxidation on Cobalt Oxide Catalysts by NAP-XPS. FTIR and XRD ACS Catal 8:8630–8641
42. Liu B, Li W, Song W, Liu J (2018) Carbonate-mediated Mars-van Krevelen mechanism for CO oxidation on cobalt-doped ceria catalysts: facet-dependence and coordination-dependence. Phys Chem Chem Phys 20:16045–59. https://doi.org/10.1039/C8CP01694A
43. Koch G, Hävecker M, Teschner D, Carey SJ, Wang Y, Kube P et al (2020) Surface Conditions That Constrain Alkane Oxidation on Perovskites. ACS Catal 10(13):7007–7020
44. Yang C, Grimaud A (2017) Factors controlling the redox activity of oxygen in perovskites: from theory to application for catalytic reactions. Catalysts 7(5):1–27. https://doi.org/10.3390/catal7050149